

Drift capability of swimming bacteria in shear flows

Fanglong Dang(党方龙), Wei Feng(冯伟), Xinlei Li(李欣蕾), Luo Hao(罗昊), Yanan Liu(刘亚楠), and Guangyin Jing(经光银)

Citation: Chin. Phys. B, 2026, 35 (**7**): 074701. DOI: 10.1088/1674-1056/ae40de
http://cpb.iphy.ac.cn; http://iopscience.iop.org/cpb

What follows is a list of articles you may be interested in

Pressure in active matter

Guo Yu(余果), Ruiyao Li(李蕤耀), Fukang Li(李富康), Jiayu Zhang(张佳玉), Xiyue Li(李西月), Zequ Chen(陈泽渠), Joscha Mecke, and Yongxiang Gao(高永祥)

Chin. Phys. B, 2025, 34 (**9**): 094702. DOI: 10.1088/1674-1056/ae030c

Flow features induced by a rod-shaped microswimmer and its swimming efficiency: A two-dimensional numerical study

Siwen Li(李斯文), Yuxiang Ying(应宇翔), Tongxiao Jiang(姜童晓), and Deming Nie(聂德明)

Chin. Phys. B, 2024, 33 (**12**): 124701. DOI: 10.1088/1674-1056/ad84c3

Gravity-capillary waves modulated by linear shear flow in arbitrary water depth

Shaofeng Li(李少峰), Jinbao Song(宋金宝), and Anzhou Cao(曹安州)

Chin. Phys. B, 2020, 29 (**12**): 124702. DOI: 10.1088/1674-1056/abb3e4

A nonlinear Schrödinger equation for gravity waves slowly modulated by linear shear flow

Shaofeng Li(李少峰), Juan Chen(陈娟), Anzhou Cao(曹安州), Jinbao Song(宋金宝)

Chin. Phys. B, 2019, 28 (**12**): 124701. DOI: 10.1088/1674-1056/ab53cf

Characteristics and generation of elastic turbulence in a three-dimensional parallel plate channel using direct numerical simulation

Hong-Na Zhang(张红娜), Feng-Chen Li(李凤臣), Xiao-Bin Li(李小斌), Dong-Yang Li(李东阳), Wei-Hua Cai(蔡伟华), Bo Yu(宇波)

Chin. Phys. B, 2016, 25 (**9**): 094701. DOI: 10.1088/1674-1056/25/9/094701

Drift capability of swimming bacteria in shear flows

Fanglong Dang(党方龙)[1], Wei Feng(冯伟)[1], Xinlei Li(李欣蕾)[2], Hao Luo(罗昊)[1], Yanan Liu(刘亚楠)[1], and Guangyin Jing(经光银)[1,†]

[1] *School of Physics, Northwest University, Xi'an* 710027, *China*
[2] *College of Life Science, Northwest University, Xi'an* 710069, *China*

(Received 11 December 2025; revised manuscript received 20 January 2026; accepted manuscript online 3 February 2026)

The ability of microorganisms to control their swimming direction is crucial for navigating complex flow environments at low Reynolds numbers. We study how swimming *Escherichia coli* generate transverse locomotion across streamlines, defined as drift swimming, i.e., perpendicular to the flow direction, resulting from the chiral coupling between their flagellar rotation and an imposed shear flow. The drift velocity increases linearly with shear rate at low shear and saturates at a maximum value comparable to the intrinsic swimming speed. This maximum drift grows monotonically as cells approach the channel wall and is strongly enhanced under geometric confinement. Reorientation dynamics reveal a marginally stable fixed point along the vorticity axis, with oscillations around it arising from thermal noise and body–flagellum misalignment. Wall-induced hydrodynamic constraints suppress these fluctuations and amplify the drift. Our results demonstrate an enhanced navigation capacity under extreme shear relevant to bacterial colonization in confined environments.

Keywords: rheotaxis, bacterial swimming, shear flow, drift motion

PACS: 47.63.Gd, 47.63.–b, 47.61.–k, 47.90.+a

DOI: 10.1088/1674-1056/ae40de **CSTR:** 32038.14.CPB.ae40de

1. Introduction

Swimming bacteria such as *Escherichia coli* propel themselves by rotating bundled helical flagella, enabling relocation, foraging, and escape from harmful conditions.[1–3] Survival depends not only on swimming fast but also on maintaining orientation in favorable directions. However, in realistic environments, directional control is challenged by fluctuations and external perturbations. Because of their small size, bacteria are highly susceptible to thermal noise, which induces rotational diffusion and continual reorientation of both the cell body and flagella. Biologically, cells counteract this loss of directionality through chemotactic signaling, adjusting their swimming direction via run-and-tumble cycles driven by coordinated flagellar rotations.[4–7] In complex media, additional nonlinear effects — such as enhanced propulsive speed from high-frequency flagellar rotation[8,9] and memory effects leading to nonpersistent motion[10–12] — further modify bacterial trajectories. Near solid boundaries, asymmetric hydrodynamic resistance generates circular motion,[13–15] continuously redirecting cells toward or along surfaces.

Unlike quiescent fluids, bacterial habitats often contain flowing liquid environments. Under flow, bacteria accumulate at walls[16–20] and even in regions of high shear.[21] Surface interactions[22,23] and hydrodynamic coupling to the background flow[24–29] can strongly regulate bacterial orientation. The bacterial body is advected by laminar flow,[30] and its orientation responds to shear similarly to elongated passive particles, which obey Jeffery's orbits. However, with self-propulsion, rod-shaped microswimmers display swinging or tumbling motions that differ fundamentally from passive rods.[31,32] Chirality further introduces transverse migration: passive chiral particles drift slowly in the vorticity direction of shear flow,[33–35] typically requiring long distances for separation to emerge.[34]

With self-propulsion, bacteria exhibit a much stronger chirality-driven drift than passive particles. This enhanced transverse migration originates from the torque exerted by shear on the rotating helical flagellar bundle,[34] which deflects the swimming direction and produces a drift velocity dependent on shear rate, chiral strength, and rotational diffusivity,[36] as well as cell aspect ratio.[37] A central theoretical prediction is that orientation along the vorticity axis is only marginally stable; cells cannot remain perfectly aligned in this direction but oscillate around it due to rotational diffusion and body–flagellum misalignment. Consequently, the drift velocity is expected to remain below the intrinsic full swimming speed. Artificial microswimmers mimicking bacterial helicity also display such oscillations in shear flow.[38] Despite these advances, the degree to which oscillations reduce the effective drift capability and the manner in which wall proximity and confinement modulate this behavior remain poorly quantified. A complete physical picture of the factors limiting the maximum drift achievable by real bacteria is still lacking.

To address this gap, we apply controlled shear flows in polydimethylsiloxane (PDMS) microfluidic channels of dif-

†Corresponding author. E-mail: jing@nwu.edu.cn

© 2026 Chinese Physical Society and IOP Publishing Ltd. All rights, including for text and data mining, AI training, and similar technologies, are reserved.

ferent heights and directly track bacterial trajectories at very high shear rates to probe the extreme limit of chirality-induced drift. Fluorescent labeling of the cell body enables quantitative measurement of the maximum drift speed, while dual labeling of both the body and flagella allows accurate determination of misalignment angles. By resolving how the maximum drift depends on channel height, we uncover the regulatory role of wall-induced hydrodynamics in suppressing rotational fluctuations and enhancing drift capability. We further demonstrate that confinement, rolling, and wobbling all contribute to modulating drift. Together, these results establish the physical mechanisms governing chiral microswimmer transport in realistic flow environments and clarify why bacteria cannot fully utilize their intrinsic swimming speed for drift.

2. Materials and methods

2.1. Bacterial culture and fluorescent labeling

Two *E. coli* strains were used in this study: *E. coli* RP437 and *E. coli* AW405. Cells were revived from frozen glycerol stocks (−80 °C) and inoculated into 10 mL of Luria–Bertani (LB) medium (1.0% tryptone, 0.5% yeast extract, 1.0% NaCl). Cultures were incubated overnight at 30 °C with shaking at 200 rpm. An aliquot of the overnight culture was diluted into fresh LB to an initial optical density of $OD_{600} \approx 0.05$ and grown for 6–7 h to the mid-exponential phase ($OD_{600} \approx 0.7$). Cells were harvested (300 rpm, 5 min), washed three times with motility buffer (10 mM potassium phosphate, 0.1 mM EDTA, 10 mM NaCl, pH 7.0), and resuspended in the same buffer for experiments. These two strains were used to serve complementary experimental purposes: RP437 was used for measurements of bacterial drift based on direct body fluorescence, thereby minimizing potential perturbations to swimming behavior, whereas AW405 was employed to enable clear visualization of flagella near surfaces.

Strain RP437 was fluorescently labeled via plasmid transformation to express yellow fluorescent protein (YFP), a widely used labeling strategy for tracking bacterial bodies in microfluidic experiments. When excited at 513 nm, cells labeled in this way emit fluorescence with a peak at 537 nm. Strain AW405 was stained with Alexa Fluor 532 (AAT Bioquest) to visualize the bacterial body and flagella simultaneously. After 6 h of growth, the culture was centrifuged and washed repeatedly with deionized water. A 500 µL aliquot of the washed suspension was mixed with 10 µL of dye and 25 µL of sodium bicarbonate, followed by incubation in the dark for 30 min at 200 rpm. Cells were washed again, resuspended in motility buffer (1 M sodium lactate, 100 mM EDTA, 1 mM L-methionine, 0.1 M potassium phosphate, pH 7.0), and adjusted to a very dilute suspension with $OD_{600} \approx 0.3$, i.e., a $\sim 0.03\%$ volume fraction, before being introduced into the microfluidic channels.

2.2. Visualization and single-cell tracking in microfluidic channels

Bacterial suspensions of fluorescently labeled *E. coli* (strains AW405 and RP437) are introduced into a PDMS microchannel driven by a syringe pump (neMESYS, 29:1 gearbox). Two channel geometries are used: the three-dimensional (3D) microchannel has a height of $H = 100$ µm, a width of $W = 600$ µm, and a length of $L = 20$ mm, while the two-dimensional (2D) microchannel has a height of $H = 8$ µm, a width of $W = 200$ µm, and a length of $L = 20$ mm, as shown in Fig. 1(a). Flow occurs in the x-direction, and the bottom and top walls correspond to $z = 0$ µm and 100 µm, respectively; $y = 0$ µm and $y = 600$ µm correspond to the right and left side walls, respectively (looking along the flow). Regarding orientation, Θ denotes the out-of-plane pitch angle relative to the x–y plane, and Ψ is the polar angle of the body–flagella axis with respect to the $-x$ direction (against the flow) in the x–y plane.

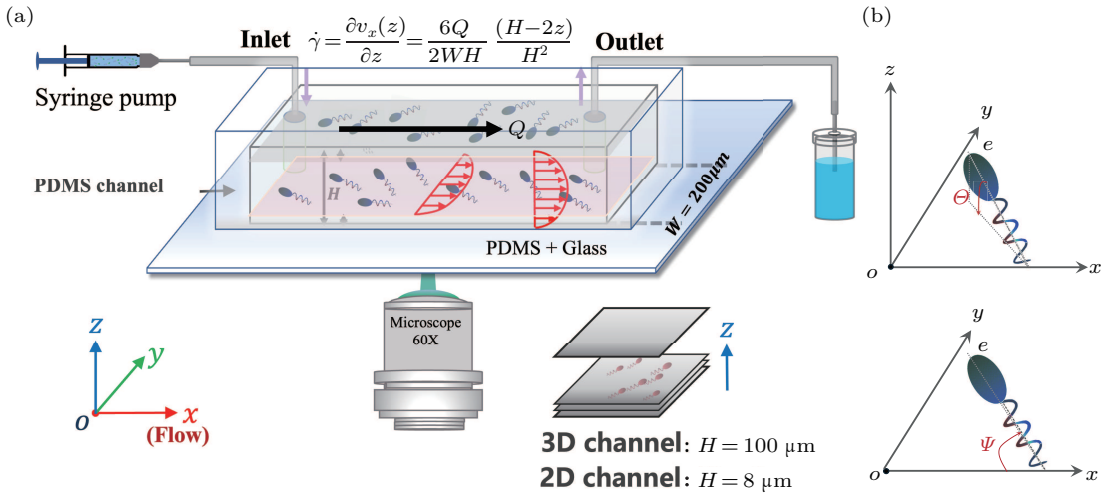


Fig. 1. Experimental setup and bacterial orientation. Bacterial suspensions were introduced into two types of microchannels at different flow rates controlled by a syringe pump.

In a shear flow, the orientation dynamics of swimming bacteria give rise to a characteristic transverse movement (in the y-direction) induced by shear along the z-direction, which we define as drift motion in the y-direction denoted by v_y. To examine the wall-regulated drift, observations were performed at multiple fixed heights from the top wall (0 to 10 μm in the 3D channel and 0 to 2 μm in the 2D channel), and at each fixed height, the local shear rate was controlled by varying the flow rate Q. Fluorescently labeled bacteria were imaged using a Nikon Ti2-E inverted microscope equipped with a 60× water-immersion objective (NA = 1.2) and a high-speed camera (Hamamatsu ORCA-Flash4.0 V3). The field of view was 225 μm × 225 μm, positioned midway between the lateral walls to minimize sidewall effects. Given the high shear rates applied, images were acquired at 100 frames per second, ensuring accurate reconstruction of rapid trajectories without motion blur or shadowing. For each recording cycle, videos were limited to 10 s to reduce photobleaching; a fresh region of the microchannel was used for subsequent recordings. Fluorescence bleaching typically reduced signal intensity by ∼ 30%, but this did not affect tracking accuracy because each dataset used newly advected cells. Single-cell positions and orientations were extracted from the fluorescence images, enabling quantification of drift velocity, flagellum–body misalignment, and height-dependent motility characteristics.

The instantaneous position (in the x–y plane) of individual bacteria (strain RP437) was detected from the recorded video stack using particle tracking velocimetry (PTV) provided by the TrackMate plugin in ImageJ. We used these instantaneous positions in the time series to calculate the drift velocity in the y-direction (transverse to the x-direction of flow) and thereby obtain the drift capability under different flows and heights. The detailed orientation of both the bacterial body and the flagellum bundle was helpful in validating the magnitude and direction of the drift motion. The instantaneous orientation of individual bacteria (strain AW405, with dyed body and flagella) was imaged via projection onto the x–y plane under different flow conditions at 1 μm above the bottom surface, as shown in Fig. 1(a). Using the orientation snapshot sequence, as shown in Fig. 1(b), the pitch and polar angle of the bacteria were analyzed using a custom tracking algorithm written in the MATLAB programming language.

3. Results

3.1. Bacterial drift velocity and saturation under high shear

Under an external flow, the shear stress exerted on the helical flagella generates a net lift force, causing swimming bacteria to deviate from the streamlines. This transverse motion, called bacterial drift, represents a chiral form of rheotaxis. To quantify this behavior, dilute suspensions of fluorescently labeled *E. coli* (strain RP437) were introduced into PDMS microchannels with a height of $H = 100$ μm, a width of $W = 600$ μm, and a length of $L = 20$ mm (Fig. 1; see Section 2 for details). The background flow velocity was measured using 1 μm dyed polystyrene microspheres, which accurately trace the local Poiseuille flow. Bacterial trajectories were recorded at a height of approximately 1 μm below the top wall.

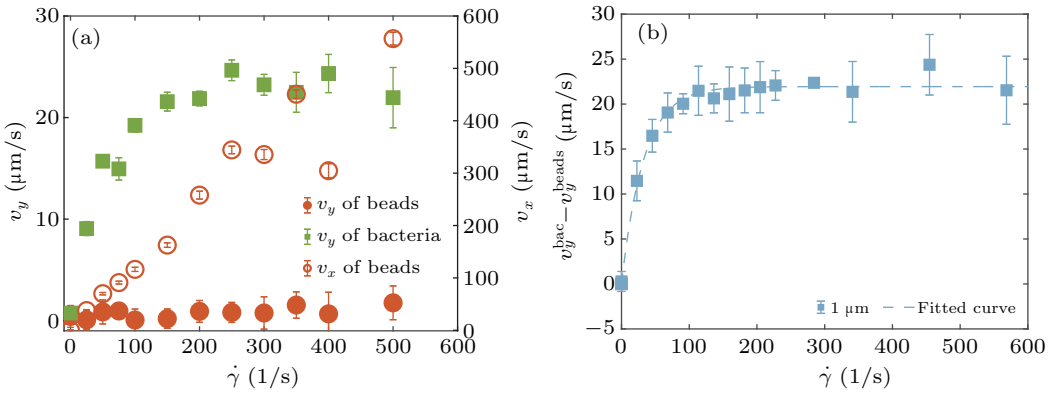


Fig. 2. Definition of bacterial drift capability. (a) Drift velocity v_y of *E. coli* strain RP437 (green squares) and tracer beads (orange circles) measured 1 μm below the top surface of a PDMS microchannel (height $H = 100$ μm and width $W = 600$ μm) under various shear rates. The difference between bacterial and tracer bead speeds represents the net drift velocity in the y-direction. The beads' velocity in the x-direction reflects the background flow velocity at the corresponding shear rate. The error bars represent the statistical variation across the bacterial population and are normalized to the square root of the sample size (i.e., the standard error of the mean). (b) Net drift velocity V_y as a function of shear rate $\dot{\gamma}$. The data represent averages from multiple independent experiments. The blue dashed line is a fit to the exponential growth function $V_y = V_y^s[1 - \exp(-\dot{\gamma}/\dot{\gamma}_c)]$, from which the maximum drift speed V_y^s and the corresponding critical shear rate $\dot{\gamma}_c$ are obtained. The error bars here and in subsequent figures represent the standard deviation (SD) of repeated experiments conducted under the same shear condition.

Since the imaging plane lies ∼ 200 μm from either lateral wall, the velocity gradient in the y-direction is negligible. The flow can therefore be written as $\boldsymbol{v} = (v_x, 0, 0)$, with a Poiseuille profile given by $v_x(z) = 4v_m(H - z)z/H^2$. The z-dependent shear rate is then $\dot{\gamma} = \partial v_x(z)/\partial z = 4v_m(H - 2z)/H^2$. Bacteria swim in this shear flow with a transverse drift in the y-direction. The maximum velocity $v_m = 3Q/(2WH)$ is obtained from the imposed flow rate Q and the dimensions of the

channel's cross-section. After extracting the net displacement of bacterial cell bodies relative to beads in the y-direction, the difference in y-coordinates between successive time points is calculated and divided by the time interval of $1/100$ second (frame rate of 100 fps) to obtain the average drift velocity of each individual bacterium. Subsequently, the drift velocities of all bacteria under the same experimental conditions are ensemble averaged. The error bars represent the statistical variation across the bacterial population and are normalized to the square root of the sample size, i.e., the standard error of the mean (green solid squares, Fig. 2(a)). As expected, the passive beads show no detectable drift at any flow strength (orange solid circles, Fig. 2(a)). In agreement with earlier measurements,[36] the bacterial drift velocity increases linearly with shear rate in the low-shear regime ($\dot{\gamma} \lesssim 20\ \mathrm{s}^{-1}$), followed by saturation at higher shear. To eliminate geometric artifacts, fluorescent beads are tracked simultaneously with bacteria (orange circles, Fig. 2(a)). The y-direction velocity of the tracer beads v_y^{beads} is subtracted from that of the bacteria v_y^{bac} to obtain the net drift velocity of the bacteria, i.e., $V_y = v_y^{\mathrm{bac}} - v_y^{\mathrm{beads}}$, and averaged over repeated experiments at each shear condition (Fig. 2(b)). The error bars here and in subsequent figures represent the standard deviation (SD) of repeated experiments conducted under the same shear condition. Fitting the data to an exponential form, $V_y = V_y^{\mathrm{s}}[1-\exp(-\dot{\gamma}/\dot{\gamma}_{\mathrm{c}})]$, yields the maximum drift velocity V_y^{s} and its characteristic shear scale $\dot{\gamma}_{\mathrm{c}}$. To quantify the drift capability of swimming bacteria, we normalize the maximum drift velocity to the intrinsic swimming speed v_0, obtained independently at the corresponding height.

3.2. Surface-driven modulation of drift velocity with distance

Having established a quantitative method for extracting drift velocity and drift capability, we next examine the influence of surfaces — critical for bacterial accumulation and contamination in confined flows. Under Poiseuille flow, the shear rate is highest near the wall; previous studies[23] have shown rich shear-induced reorientation dynamics. However, the height dependence of the normalized drift velocity and drift capability has remained unknown. We tracked swimming bacteria at different distances from the top wall at various shear rates and extracted the corresponding drift velocities. The drift velocity component associated with self-propulsion is $V_y = v_0 \sin(\Psi)\cos(\Theta)$. The self-propulsion speed v_0, determined by flagellar propulsion, varies between individual cells but remains approximately constant on average across different flow conditions. The normalized drift velocity V_y/v_0 is shown in Fig. 3(a). In the linear regime, the normalized drift velocity scales linearly with shear rate, $V_y/v_0 \sim l_0\dot{\gamma}/v_0$ with $l_0 \approx 0.1 v_0 \nu / D_{\mathrm{r}}^{\mathrm{eff}}$ comparable to the bacterial body length.[36]

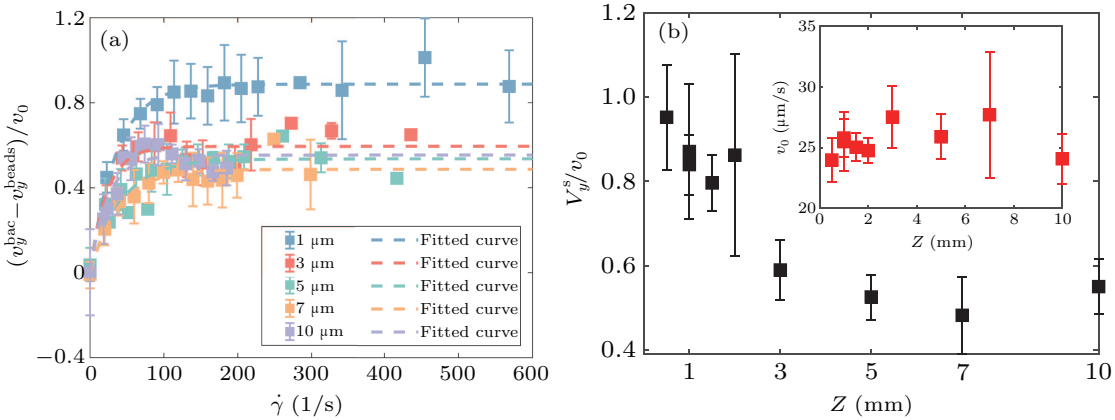


Fig. 3. Bacterial drift capability versus distance from the wall. (a) The normalized drift velocity is obtained by dividing the measured drift velocities by the self-propulsion speed v_0. At each height, the normalized drift velocity increases with shear and saturates at high values. Its slope versus shear decreases rapidly within the first 5 μm from the wall and gradually levels off farther away. (b) Drift capability V_y^{s} as a function of height, showing a sharp decay within 5 μm and a constant value above this range. The values of V_y^{s} are obtained by fitting the measured v_y–$\dot{\gamma}$ data using the exponential growth function $V_y = V_y^{\mathrm{s}}[1-\exp(-\dot{\gamma}/\dot{\gamma}_{\mathrm{c}})]$. The inset shows that the self-propulsion speed v_0 is approximately constant with height.

Based on Fig. 3(a), we extracted the maximum drift velocity and normalized it to the self-propulsion speed v_0 to quantify the drift capability. The resulting drift capability V_y^{s}/v_0 decreases systematically with height and reaches a constant value approximately 5 μm away from the wall (Fig. 3(b)). Within this near-wall region, V_y^{s}/v_0 increases as bacteria approach the wall; beyond it, the surface influence becomes negligible. As bacteria approach the wall, their alignment becomes more parallel to the surface,[23] reducing their effective rotational diffusion $D_{\mathrm{r}}^{\mathrm{eff}}$. This reduction enhances the drift velocity within the near-wall region, consistent with the height-dependent trend observed in Fig. 3, which is discussed in detail in the following section.

3.3. Drift motion from 3D to 2D confinement

Our measurements show that bacterial drift capability is strongly enhanced near solid boundaries. This motivates us to examine how confinement further modulates drift, given

its well-known influence on microswimmer dynamics.[39–42] To this end, we introduced bacterial suspensions into a quasi-two-dimensional microchannel with a height of 8 μm. As shown in Fig. 4(a), the maximum drift velocity decreases with increasing distance from the top wall, similar to the trend in three-dimensional channels, but with higher absolute values under confinement. This enhancement is consistent with the strong hydrodynamic resistance imposed by bounding surfaces, which suppresses orientational wobbling and other oscillatory components of bacterial motion.[41]

The normalized drift velocity in the two-dimensional channel (Fig. 4(b)) also exceeds that measured in three dimensions. Remarkably, the normalized drift can exceed unity, suggesting that under high shear, the swimming speed of bacteria may increase due to the extra load on the flagellar motor;[43] however, it is challenging to directly measure this speed under strong shear. The swimming speed v_0 used to obtain V_y^s/v_0 was measured under quiescent conditions in our experiments. This flow-response enhancement of swimming speed might be underestimated here, leading to a drift velocity larger than the full speed of the bacteria, specifically $V_y^s/v_0 > 1$. This observation highlights the need for more precise measurements to understand the biological and mechanical responses of motile bacteria to confined and strongly sheared environments.

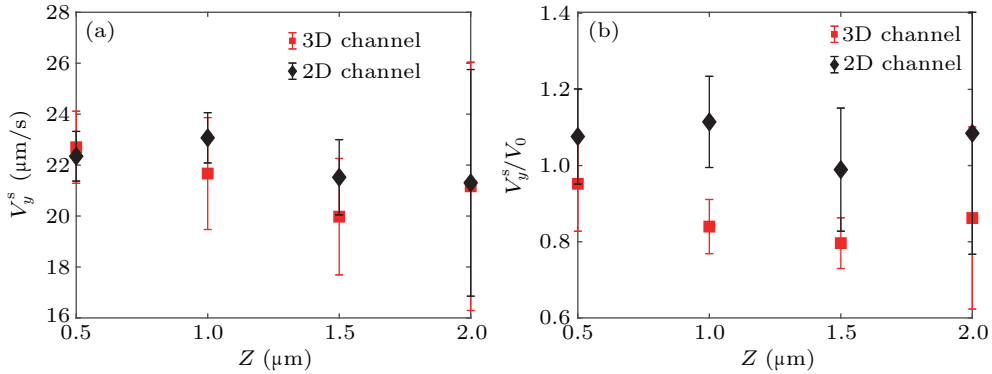


Fig. 4. Confinement-enhanced drift capability. (a) Maximum drift speed as a function of height in 2D and 3D channels. In both geometries, the drift decreases with distance from the top wall but remains systematically higher under 2D confinement. (b) Maximum drift speed normalized by the intrinsic swimming speed at each height, confirming the pronounced enhancement of drift capability in the 2D channel.

3.4. Drift with rolling motion on surfaces

When bacteria swim near a solid boundary under flow, the no-slip condition creates a strong velocity gradient normal to the surface. The resulting shear induces a rolling motion in which the bacterium rotates around a near-contact point on the wall, as illustrated in Fig. 5(a). To resolve this process, we fluorescently labeled the flagellar bundles (strain AW405). Although this labeling slightly reduces propulsion efficiency, it enables direct visualization of body–flagellum dynamics.

Near the surface, the cell body and flagella counter-rotate, generating hydrodynamic torques of the same sign at the interface. These interactions drive circular motion and produce an approximately uniform in-plane orientation distribution in the absence of flow, as shown in Fig. 5(b).[13–15] As the shear rate increases (e.g., $\dot{\gamma} = 30\ \mathrm{s}^{-1}$), cells progressively orient against the flow through the combined action of the weathervane effect and surface-induced drift, driving Ψ toward 90°. However, even at higher shear ($\dot{\gamma} = 60\ \mathrm{s}^{-1}$), a fraction of cells fails to reach full cross-stream alignment, causing the drift velocity to remain below the intrinsic swimming speed.

Flagellar imaging further reveals that the bundle is rarely aligned with the body axis under either quiescent or flow conditions. We define the misalignment between the body axis and bundle axis as the off-axis angle θ_{off} [Fig. 5(c)]. The frequency of changes in θ_{off} increases slightly under stronger shear, consistent with the enhanced rolling near the surface. It has been reported that off-axis configurations strongly influence bacterial motility:[11] when the flagellar bundle is aligned, counter-rotation of the body and flagella (ω_{b} and ω_{t}) balances, yielding straight swimming. When off-axis, this balance requires an additional compensatory torque ω_{cm}, generating wobbling motion — helical trajectories in 3D and zigzag paths in the imaging plane. This wobbling reduces the effective swimming speed and introduces periodic fluctuations in orientation, thereby modifying the net drift capability near surfaces.

4. Discussion

The experimental results demonstrate that bacteria drift across flow due to chirality-induced rheotaxis; under sufficiently strong shear, they can reach a saturated drift velocity comparable to their intrinsic swimming speed. The maximum drift capability depends on multiple factors, including shear strength, wall effects, wobbling dynamics, and orientation fluctuations driven by thermal noise or run-and-tumble randomization. We find that the maximum drift velocity is approached once the shear rate exceeds a critical value and that this maximum decreases with distance from the wall. Under confinement, bacteria at the same wall distance exhibit even higher maximum drift speeds than those in 3D environments. In the following, we discuss the mechanism behind these experimental observations.

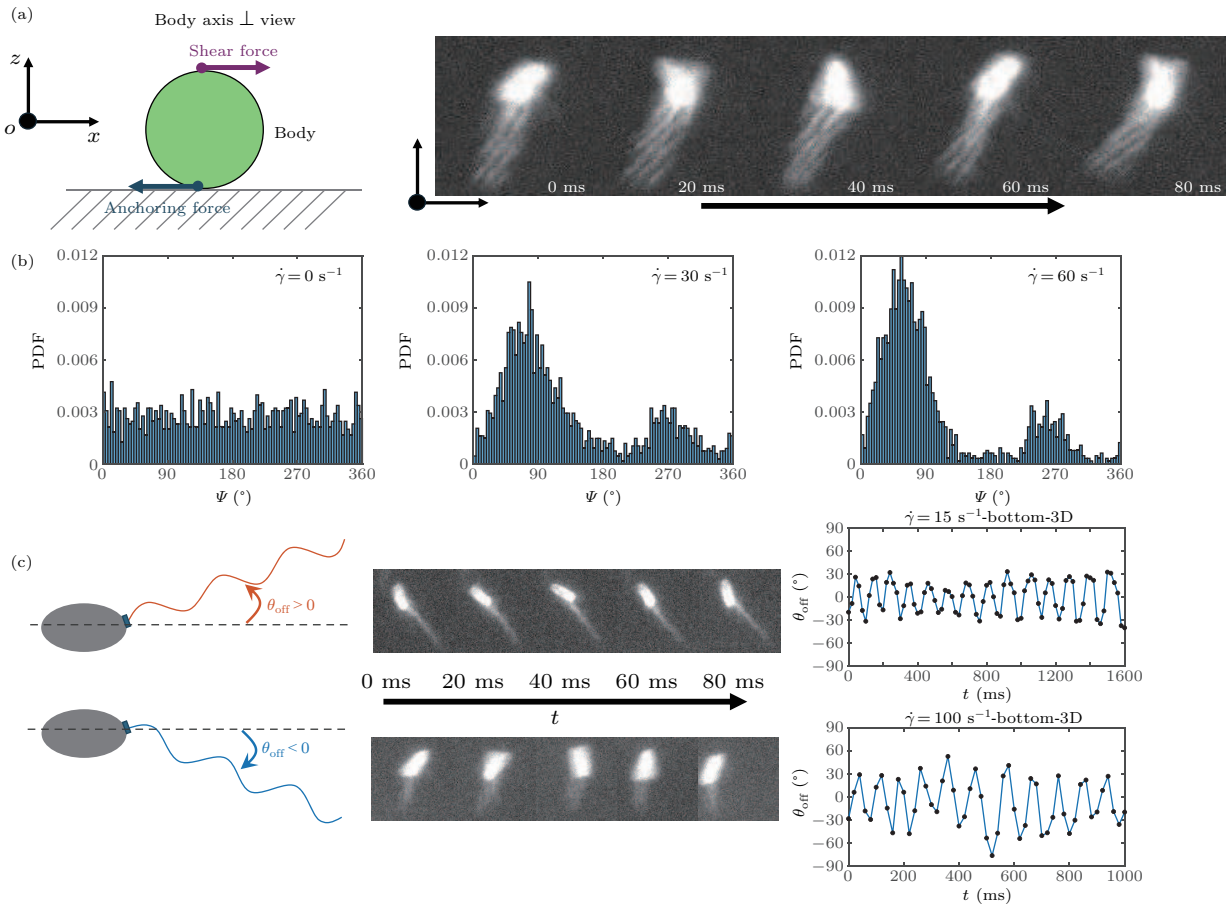


Fig. 5. Rolling motion modulates bacterial drift near surfaces. (a) Near a no-slip boundary, the velocity gradient in the z-direction generates a shear-induced torque. Relative motion between the bacterium and the surface produces an anchoring force and a corresponding anchoring torque. Together, these torques drive the rolling motion of the cell body along the interface (left). Under shear, partially splayed flagellar bundles exhibit reduced propulsive efficiency, diminishing the net drift capability (right). (b) Biological variability leads to heterogeneous drift torques and thus a broad distribution of Ψ. With increasing shear ($\dot{\gamma} = 30\ \mathrm{s}^{-1}$), cells tend to orient against the flow, pushing Ψ toward 90°. Even at higher shear ($\dot{\gamma} = 60\ \mathrm{s}^{-1}$), full cross-stream alignment is not achieved for all cells, and some exhibit reverse drift, collectively reducing the population-averaged drift speed. (c) The off-axis angle θ_{off} — defined as the angle between the cell body axis and the flagellar bundle axis, positive for counterclockwise and negative for clockwise rotation — oscillates periodically over time. Higher shear slightly increases the frequency of these $\pm\alpha$ oscillations due to enhanced rolling near the surface. Such persistent off-axis motion continually perturbs the three-dimensional orientation of bacteria, further weakening their drift capability at the interface.

4.1. Drift motion saturates below the full swimming speed

The translational and orientational dynamics of a bacterium in a flat channel follow[23,36]

$$\frac{\mathrm{d}\boldsymbol{r}}{\mathrm{d}t} = v_0\boldsymbol{e} + v_x(z) + \mathcal{H}\cdot\boldsymbol{\xi}, \tag{1}$$

$$\frac{\mathrm{d}\boldsymbol{e}}{\mathrm{d}t} = \left[\boldsymbol{\Omega}_{\mathrm{J}} + \boldsymbol{\Omega}_{\mathrm{C}} + \sqrt{2D_{\mathrm{r}}}\boldsymbol{\xi}_{\mathrm{r}}\right]\times\boldsymbol{e}, \tag{2}$$

where $\boldsymbol{r}$ is the center-of-mass position and $\boldsymbol{e} = (-\cos\Theta\cos\Psi,\ \cos\Theta\sin\Psi,\ \sin\Theta)$ is the orientation. Here, $\boldsymbol{\xi}$ and $\boldsymbol{\xi}_{\mathrm{r}}$ denote zero-mean Gaussian white noises representing translational and rotational fluctuations, respectively, with uncorrelated components ($\langle\xi_i\xi_j\rangle = \langle\xi_i^r\xi_j^r\rangle = \delta_{ij}$ for $i,j = x,y,z$), $\mathcal{H}$ is the anisotropic diffusion tensor, and D_{r} is the rotational diffusion.[44] The Jeffery reorientation rate $\boldsymbol{\Omega}_{\mathrm{J}}$ describes the hydrodynamics of elongated particles,[45–48] with components $\Omega_{\mathrm{J}}^x = (\dot{\gamma}/2)Ge_xe_y$, $\Omega_{\mathrm{J}}^y = (\dot{\gamma}/2)\left[1+G(e_z^2-e_x^2)\right]$, and $\Omega_{\mathrm{J}}^z = -(\dot{\gamma}/2)Ge_ye_z$, where $G = (\alpha^2-1)/(\alpha^2+1) \lesssim 1$ is the Bretherton constant and α is the aspect ratio. Chirality induces an additional reorientation,[23,36] $\Omega_{\mathrm{C}}^x = -\nu\dot{\gamma}e_z(2e_x^2-1)$, $\Omega_{\mathrm{C}}^y = -2\nu\dot{\gamma}e_xe_ye_z$, $\Omega_{\mathrm{C}}^z = -\nu\dot{\gamma}e_x(2e_x^2-1)$, with ν being the chiral strength.

In the noiseless limit,[36] the orientation dynamics reduce to

$$\begin{pmatrix}\dot{\Psi}\\ \dot{\Theta}\end{pmatrix} = \begin{pmatrix}(\dot{\gamma}/2)(1+G)\sin\Psi\tan\Theta + \dot{\gamma}\nu\cos\Psi\dfrac{\cos 2\Theta}{\cos\Theta}\\ -(\dot{\gamma}/2)(1-G\cos 2\Theta)\cos\Psi + \dot{\gamma}\nu\sin\Psi\sin\Theta\end{pmatrix}. \tag{3}$$

Solving Eq. (3) shows that $(\Psi^* = \pm\pi/2, \Theta^* = 0)$ are fixed points, implying that bacteria ultimately drift perpendicular to the flow. Linearizing at these points yields the Jacobian with determinant $\Delta = -(\dot{\gamma}^2/4)(4\nu^2+G^2-1) > 0$, and trace $\tau = 0$. Since $\nu \sim 0.1$ and $G < 1$, the eigenvalues are $\lambda_{1,2} = \pm\mathrm{i}(\dot{\gamma}/2)\sqrt{1-G^2-4\nu^2} = \pm\mathrm{i}\omega$, indicating that the fixed point is marginally stable. Consequently, the approach to $\Psi^* = \pi/2$ is extremely slow, and the drift force vanishes as the orientation saturates, yielding the observed plateau in drift speed. The remaining question is why this plateau is always below the full swimming speed.

4.2. Orientation fluctuations induced by noise

Because bacteria are micron-sized, rotational diffusion plays a crucial role. In bulk, even extremely weak noise generates oscillations around $\Psi^* = \pi/2$ at high shear.[36,38] In our experiments, the maximum drift velocity increases sharply near the wall. As the drift force becomes vanishingly small near the fixed point, noise dominates the dynamics.

Hydrodynamic interactions near the wall substantially enhance friction for a rod at a distance d from the surface.[49,50] The transverse friction coefficient scales as $\xi_\perp = \xi_{\infty,\perp}\left[1+\left(0.090+0.097(1-\cos\theta)^4\right)(D/d)\right]$, so that the rotational diffusion $D_\mathrm{r} = k_\mathrm{B}T/\xi_\perp$ decreases as the rod approaches the surface. Under even stronger confinement, simulations show a continuous reduction in D_r as the wall separation decreases.[51] In our system, reduced rotational diffusion near the wall suppresses noise-driven oscillations around $\Psi^* = \pi/2$, thereby enhancing the maximum drift capability. Under quasi-2D confinement, rotational diffusion decreases further, consistent with the even larger maximum drift velocity observed experimentally.

4.3. Wobbling reduces drift capability

A flagellated bacterium is often modeled as two spheres connected by a rod, implicitly assuming that the cell body and flagellar axes are collinear. In reality, they are misaligned, producing a torque imbalance that causes wobbling along a helical path and reduces the net swimming speed.[11] Because drift velocity is defined as the component of swimming velocity perpendicular to the flow, wobbling necessarily reduces the effective drift.

A model swimmer consisting of a spherical body and a helical flagellum joined at a fixed angle[52] shows that even weak misalignment substantially modifies drift behavior. Thus, under large shear, wobbling generates periodic oscillations around $\Psi^* = \pi/2$ and lowers the maximum drift speed. Experiments further show that the wobbling amplitude decreases in a colloidal suspension with viscosity η, where a boundary-induced torque adjusts the wobbling angle θ according to $-K(\theta-\theta_0) = (\pi/5)\,\eta\, r_\mathrm{b}^2 V_\mathrm{b}\,\gamma(17+8\gamma)/(1+\gamma)^2\,\ln[r_\mathrm{b}(1+\gamma)/(2d)]$, where K is the hook bending stiffness, $\gamma = R/r_\mathrm{b}$ is the size ratio between the colloid and the bacterium, and d is the minimum surface separation.[11] As the effective colloid radius grows, wobbling is strongly suppressed. A wall acts as an effectively infinite colloid, so bacteria near the interface wobble less, reducing orientation oscillations around $\Psi^* = \pi/2$ and thereby enhancing the maximum drift. In confinement, the wobbling amplitude decreases even further,[40,53] which is consistent with the enhanced drifting capability observed in quasi-2D channels.

5. Conclusions

In summary, we have systematically quantified the drift behavior of swimming *E. coli* in both 3D and strongly confined 2D microchannels. The drift velocity and drift capability remain well below the intrinsic swimming speed, yet both increase markedly as cells approach solid boundaries. This enhancement originates from wall-induced suppression of rotational diffusion and wobbling, which stabilizes the bacterial orientation toward the drift-favorable direction. Confinement further amplifies this effect by restricting motion to a quasi-two-dimensional geometry, leading to a pronounced increase in drift capability. Additional factors, such as rolling near surfaces, also modulate the observed drift. These results clarify how hydrodynamic interactions and confinement shape the transverse transport of chiral microswimmers, offering fundamental insights into bacterial navigation in complex and confined environments.

Acknowledgments

Project supported by the National Natural Science Foundation of China (Grant Nos. 12174306, 12004308, W2421001, and 12474197), the Natural Science Basic Research Program of Shaanxi (Grant Nos. 2023-JC-JQ-02 and 2024JC-ZDXM-06), the Shaanxi Academy of Fundamental Sciences (Mathematics, Physics No. 23JSY024), and Shaanxi Province Science and Technology Rising Star Program (Grant No. 2025ZC-KJXX-51).

References

[1] Hölscher T, Bartels B, Lin Y C, Gallegos-Monterrosa R, Price-Whelan A, Kolter R, Dietrich L E P and Kovács Á T 2015 *J. Mol. Biol.* **427** 3695
[2] Watteaux R, Stocker R and Taylor J R 2015 *J. Theor. Biol.* **387** 120
[3] Toews M L, Goy M F, Springer M S and Adler J 1979 *Proc. Natl. Acad. Sci. USA* **76** 5544
[4] Berg H C 1975 *Annu. Rev. Biophys. Bioeng.* **4** 119
[5] Chamolly A and Lauga E 2020 *Phys. Rev. Fluids* **5** 123102
[6] Berg H C and Brown D A 1972 *Nature* **239** 500
[7] Dvoriashyna M and Lauga E 2021 *PLoS One* **16** e0254551
[8] Zöttl A and Yeomans J M 2019 *Nat. Phys.* **15** 554
[9] Qu Z and Breuer K S 2020 *Phys. Rev. Fluids* **5** 073103
[10] Patteson A E, Gopinath A, Goulian M and Arratia P E 2015 *Sci. Rep.* **5** 15761
[11] Kamdar S, Shin S, Leishangthem P, Francis L F, Xu X and Cheng X 2022 *Nature* **603** 819
[12] Cao X, Das D, Windbacher N, Ginot F, Krüger M and Bechinger C 2023 *Nat. Phys.* **19** 1904
[13] Lauga E, DiLuzio W R, Whitesides G M and Stone H A 2006 *Biophys. J.* **90** 400
[14] Giacché D, Ishikawa T and Yamaguchi T 2010 *Phys. Rev. E* **82** 056309
[15] Lopez D and Lauga E 2014 *Phys. Fluids* **26** 071902
[16] Berke A P, Turner L, Berg H C and Lauga E 2008 *Phys. Rev. Lett.* **101** 038102
[17] Li G and Tang J X 2009 *Phys. Rev. Lett.* **103** 078101
[18] Sartori P, Chiarello E, Jayaswal G, Pierno M, Mistura G, Brun P, Tiribocchi A and Orlandini E 2018 *Phys. Rev. E* **97** 022610
[19] Li G, Bensson J, Nisimova L, Munger D, Mahautmr P, Tang J X, Maxey M R and Brun Y V 2011 *Phys. Rev. E* **84** 041932

[20] Xu X X, Tian Y, Pu Y, Che B, Luo H, Liu Y, Liu Y J and Jing G 2025 *J. Phys. Chem. B* **129** 2647
[21] Rusconi R, Guasto J S and Stocker R 2014 *Nat. Phys.* **10** 212
[22] Tung C K, Ardon F, Roy A, Koch D L, Suarez S S and Wu M 2015 *Phys. Rev. Lett.* **114** 108102
[23] Mathijssen A J T M, Figueroa-Morales N, Junot G, Clément É, Lindner A and Zöttl A 2019 *Nat. Commun.* **10** 3434
[24] Nash R W, Adhikari R, Tailleur J and Cates M E 2010 *Phys. Rev. Lett.* **104** 258101
[25] Mathijssen A J T M, Shendruk T N, Yeomans J M and Doostmohammadi A 2016 *Phys. Rev. Lett.* **116** 028104
[26] Figueroa-Morales N, Rivera A, Soto R, Lindner A, Altshuler E and Clément É 2020 *Sci. Adv.* **6** eaay0155
[27] Hill J, Kalkanci O, McMurry J L and Koser H 2007 *Phys. Rev. Lett.* **98** 068101
[28] Figueroa-Morales N, Miño G L, Rivera A, Caballero R, Clément E, Altshuler E and Lindner A 2015 *Soft Matter* **11** 6284
[29] Zöttl A 2020 *Chin. Phys. B* **29** 074701
[30] Kaya T and Koser H 2009 *Phys. Rev. Lett.* **103** 138103
[31] Li R, Gompper G and Ripoll M 2021 *Macromolecules* **54** 812
[32] Rost B, Stimatze J T, Egolf D A and Urbach J S 2020 *Phys. Rev. E* **102** 023103
[33] Makino M, Arai L and Doi M 2005 *Phys. Fluids* **17** 103605
[34] Marcos, Fu H C, Powers T R and Stocker R 2009 *Phys. Rev. Lett.* **102** 158103
[35] Makino M, Arai L and Doi M 2008 *J. Phys. Soc. Jpn.* **77** 064404
[36] Jing G, Zöttl A, Clément É and Lindner A 2020 *Sci. Adv.* **6** eabb2012
[37] Zhong J and Xu X 2025 *Phys. Fluids* **37** 021707
[38] Zöttl A, Tesser F, Matsunaga D, Laurent J, Du Roure O and Lindner A 2023 *Proc. Natl. Acad. Sci. USA* **120** e2310939120
[39] Ping L, Wasnik V and Emberly E 2014 *FEMS Microbiol. Ecol.* **91** 1
[40] Yin Y, Yu H T, Tan H, Cai H, Chen H Y, Lo C J and Guo S 2022 *Biophys. J.* **121** 4656
[41] Vizsnyiczai G, Frangipane G, Bianchi S, Saglimbeni F, Dell'Arciprete D and Di Leonardo R 2020 *Nat. Commun.* **11** 2340
[42] Yan N, Xie C, Luo H, Liu Y and Jing G 2023 *Chin. Phys. B* **32** 114704
[43] Niu Y, Zhang R and Yuan J 2023 *Sci. Adv.* **9** eadi6724
[44] Drescher K, Dunkel J, Cisneros L H, Ganguly S and Goldstein R E 2011 *Proc. Natl. Acad. Sci. USA* **108** 10940
[45] Bretherton F P and Rothschild N M V 1961 *Proc. R. Soc. B* **153** 490
[46] Junot G, Figueroa-Morales N, Darnige T, Lindner A, Soto R, Auradou H and Clément E 2019 *Europhys. Lett.* **126** 44003
[47] Ezhilan B and Saintillan D 2015 *J. Fluid Mech.* **777** 482
[48] Zöttl A and Stark H 2013 *Eur. Phys. J. E* **36** 4
[49] Padding J T and Briels W J 2010 *J. Chem. Phys.* **132** 054511
[50] Yang Y and Bevan M A 2017 *J. Chem. Phys.* **147** 054902
[51] Neild A, Padding J T, Yu L, Bhaduri B, Briels W J and Ng T W 2010 *Phys. Rev. E* **82** 041126
[52] Marcos, Fu H C, Powers T R and Stocker R 2012 *Proc. Natl. Acad. Sci. USA* **109** 4780
[53] Cheon J, Son J, Lim S, Jeong Y, Park J H, Mitchell R J, Kim J U and Jeong J 2024 *Soft Matter* **20** 7313